

Superconducting properties and hydrostatic pressure effect on ABi_3 (A = Ba, Sr) single crystals

Rajveer Jha, Marcos A. Avila and Raquel A. Ribeiro

CCNH, Universidade Federal do ABC (UFABC), Santo André, SP, 09210-580 Brazil

We report on the crystal growth and characterization of ABi_3 (A = Ba, Sr) superconductors. Single crystals of both compounds were grown by the self-flux technique. $BaBi_3$ crystallized in a tetragonal structure with space group $P4/mmm$ and $SrBi_3$ in a cubic structure with space group $Pm-3m$. Superconductivity at $T_c = 6.0$ K for $BaBi_3$ and $T_c = 5.6$ K for $SrBi_3$ have been confirmed through dc magnetic susceptibility and electrical transport measurements. The dc magnetic susceptibility under hydrostatic pressure shows a positive pressure coefficient of $dT_c/dP = 1.22$ K/GPa for $BaBi_3$ and a negative pressure coefficient of $dT_c/dP = -0.48$ K/GPa for $SrBi_3$. The normal state electrical resistivity shows that both compounds are highly metallic in nature. The upper critical fields H_{c2} evaluated by resistivity under magnetic fields $\rho(T, H)$ are 22 kOe for $BaBi_3$ and 2.9 kOe for $SrBi_3$. A specific heat jump of $\Delta C/\gamma T_c = 1.05$ suggests weak coupling superconductivity in $BaBi_3$, whereas $\Delta C/\gamma T_c = 2.08$ for $SrBi_3$ is higher than the BCS theory value of 1.43, indicating a strong coupling superconductor.

Key words: Superconductors, alkaline earth bismites, critical fields, hydrostatic pressure.

*Corresponding Authors

Prof. Dr. Raquel A. Ribeiro
raquel.ribeiro@ufabc.edu.br
and
Dr. Rajveer Jha,
rajveerjha@gmail.com

Introduction

Bismuth is a very interesting element for condensed matter physics due to its electronic behavior: low carrier density, small effective mass, high mobility, long mean free path, and a large g -factor. Because of such interesting electronic properties, bismuth plays an important role in the discovery of new superconducting compounds such as the topological superconductors Bi_2X_3 (X=Se, Te), $Bi_4O_4S_3$, $REO_{1-x}F_xBiS_2$ (RE=La, Ce, Nd, and Pr) and others [1-7]. Despite having already been studied in the past, Bi-rich superconductors ABi_3 (A = Ba, Sr) have attracted

renewed attention in recent times. The older studies on these materials resulted rather limited in depth, probably due to their rather complex synthesis and air sensitivity. However, the superconductivity was reported in 1952 for polycrystalline ABi_3 by Matthias and Hulm [8]. Recently, various research groups have reported the superconducting properties of ABi_3 for single crystalline compounds [9-11]. In these reports, heat capacity analysis suggested that BaBi_3 with superconducting transition $T_c = 5.9$ K is a weakly coupled superconductor whereas SrBi_3 with $T_c = 5.75$ K is a strongly coupled superconductor. Theoretically, it has been suggested that BaBi_3 is a 3D-metal and the Bi p -bands are dominant at the Fermi level, resulting in a complex Fermi surface [9]. In addition, a comparatively large mass enhancement has been proposed for SrBi_3 , in which the Bi-6 p electrons are the essential contributors to the Fermi surface [10]. Interestingly, the T_c has been increased to 9.0 K with Na doping in SrBi_3 obtained by a high-pressure and low-temperature synthesis technique [12]. The authors interpret the increase as a result of tuning the number of valence electrons, but disregard the effect of chemical pressure. However, external physical pressure (P) plays a significant role on the T_c of most metallic and intermetallic superconductors [13-20]. Generally, the applied pressure can change the electronic structure, phonon frequencies and/or electron-phonon coupling, all of which will affect T_c and result in positive or negative pressure coefficients (dT_c/dP) [13-20]. Therefore, it was deemed worthwhile to apply hydrostatic pressure on these compounds and follow the effect on their superconducting properties.

In this work, we report on the synthesis and superconducting properties of ABi_3 ($A = \text{Ba}, \text{Sr}$) single crystals, obtained by the self-flux growth method. BaBi_3 crystallized in a tetragonal structure with space group $P4/mmm$, and SrBi_3 crystallized in a cubic structure with space group $Pm-3m$. Magnetic susceptibility and electrical transport measurements confirmed that BaBi_3 becomes superconducting below 6 K, which is slightly higher than the earlier reported value of 5.6 K [8], and SrBi_3 is a superconductor below 5.6 K. Both compounds are highly metallic based on normal state electrical resistivity measurements, and the calculated upper critical fields (H_{c2}) through resistivity under magnetic field $\rho(T)|_H$ data are 22 kOe for BaBi_3 and 2.9 kOe for SrBi_3 . Heat capacity measurements for the studied BaBi_3 suggests weakly coupled superconductivity, whereas SrBi_3 is a strongly coupled superconductor. The dc magnetic susceptibility under hydrostatic pressure for BaBi_3 reveals a positive pressure coefficient of $dT_c/dP = 1.22$ K/GPa, and a negative pressure coefficient $dT_c/dP = -0.48$ K/GPa for SrBi_3 . These are the first reports of

superconductivity under hydrostatic pressure on ABi_3 (A=Ba and Sr) superconducting compounds.

Experimental Details

Single crystalline samples of ABi_3 (A=Ba, Sr) were prepared through Bi-self flux technique. Ba, Sr pieces (99.95%, Alfa Aesar) and Bi pieces (99.99%, Alfa Aesar) with molar ratio 1:4 were weighed in an Ar-filled glove box then sealed in an evacuated quartz tube. The sealed quartz tubes were slowly heated to 600 °C and dwelled for 10 hours, then slowly cooled down to 350 °C at 2 °C/h. Finally, the quartz tubes were inverted and quickly spun into a centrifuge to remove the excess Bi flux. Rectangular single crystals with shining surfaces and sizes about $1.5 \times 1.5 \times 1.0 \text{ mm}^3$ were obtained [see Fig. 1]. The single crystals are air-sensitive and thus they were kept inside the glove box until characterization, to avoid decomposition of the samples. Room temperature X-ray diffraction (XRD) patterns were taken with $\text{CuK}_{\alpha 1}$ radiation ($\lambda = 1.54 \text{ \AA}$) using a STOE STADI-P powder diffractometer in transmission geometry. Heat capacity and electrical transport properties were measured on a Quantum Design physical properties measurement system (PPMS-14T) and magnetic properties measurements were performed on a Quantum Design magnetic property measurement system (MPMS3-7T). The dc magnetic susceptibility under pressure was measured by using a nonmagnetic Cu-Be cylindrical hydrostatic pressure cell in a pressure range up to 1.3 GPa on the MPMS3. We used Daphne oil 7373 as a liquid pressure transmitting medium and a small piece of tin (Sn) was used as a pressure manometer. An uncertainty in pressure of the order $P \sim \pm 0.05 \text{ GPa}$ was determined from the width of the superconducting transition of the Sn manometer.

Results and discussion

Figure 2 illustrates Rietveld refined powder x-ray diffraction patterns at room temperature for ABi_3 (A=Ba, Sr). We grouped many small and randomly oriented pieces of single crystals to take the XRD data, and recorded the 2θ sweep in fast mode with a rate of $4^\circ/\text{min}$ to avoid the decomposition of the samples. The BaBi_3 crystallized in a tetragonal structure (distorted AuCu_3 structure) with space group $P4/mmm$. The refined lattice parameters are $a = 5.06(1) \text{ \AA}$ and $c = 5.13(2) \text{ \AA}$. In contrast, SrBi_3 crystallized in a cubic structure (AuCu_3)

with space group $Pm-3m$ and a refined lattice parameter $a = 5.05(3)$ Å. The resultant lattice parameters are in good agreement with earlier reported results [8-12]. The unit cell for ABi_3 is shown in Fig. 2b, resembling a $AuCu_3$ structure with Bi_6 octahedra.

Figure 3a shows the temperature dependent dc magnetic susceptibility of $BaBi_3$ under an applied magnetic field $H = 10$ Oe. The magnetic susceptibility measurements were taken using two protocols: Zero Field Cooled (ZFC) and Field Cooled (FC). A sharp diamagnetic transition at 6 K testifies the high quality of the $BaBi_3$ single crystal. A large diamagnetic signal is observed below 6 K in the ZFC curve. The value of $4\pi\chi$ (ZFC) at 2 K exceeds -1 , indicating that the shielding volume fraction at 2 K is essentially 100% and implies bulk superconductivity in the $BaBi_3$ single crystal. The 5-quadrant isothermal magnetization loop ($M \times H$) at 2.1 K for $BaBi_3$ is shown in inset of Fig. 3a. A clear hysteresis is observed, which indicates a typical type-II superconducting behavior. As the magnetic field increases from zero, the magnetization decreases linearly up to $H_{c1} = 400$ Oe (at 2.1 K). Above H_{c1} , the magnetization starts increasing, reaches zero and becomes positive above an applied field of 14 kOe, i.e., the H_{c2} estimated through magnetization is comparably high in this compound. Fig. 3b presents the lower critical fields (H_{c1}) as a function of T/T_c . For a superconductor the critical fields at absolute zero temperature provide important thermodynamic information. The lower critical field of $BaBi_3$ at absolute zero temperature has been estimated by fitting the equation $H_{c1}(T) = H_{c1}(0)[1 - (T/T_c)^2]$ (solid red line) to the values extracted from the magnetization curves between 2.1 K – 5 K (inset of Fig. 3b). A similar behavior observed for higher temperatures as long as the sample is in the superconducting state, i.e. below 6 K. The estimated critical fields are $H_{c1}(0) = 1.71$ kOe and $H_{c2}(0) = 14.7$ kOe. The large $H_{c2}(0)$ implies a small superconducting coherence length of $\xi_0 = 149$ Å, according to $H_{c2}(0) = \Phi_0/2\pi\xi_0^2$, where $\Phi_0 = 2.0678 \times 10^9$ Oe.Å² [21]. The thermodynamic critical field $H_c(0)$ can be calculated as the arithmetic mean of the upper and lower critical fields at absolute zero temperature, i.e. $H_c = (H_{c1}H_{c2})^{1/2}$, and the resulting value is 5.02 kOe. In the Meissner state, using Ginzburg–Landau theory the upper critical field and thermodynamic critical field are related by $H_{c2} = 2^{1/2}\kappa H_c$. The Ginzburg–Landau parameter κ thus estimated is $2.07 > 1/2^{1/2}$, implying type-II superconductivity in $BaBi_3$ [21]. Further, the penetration depth $\lambda(0)$ is calculated from the relation $\lambda(0) = \kappa\xi(0)$, which results in 309 Å.

The $\chi \times T$ curves in ZFC and FC mode under $H = 10$ Oe shows a clear and sharp diamagnetic transition onset around 5.6 K for the SrBi₃ single crystal (Fig. 4a). The hysteresis between ZFC and FC regimes indicates SrBi₃ is a type II superconductor. Without correcting for demagnetization or sample size effects, we estimate the superconducting volume fraction (ZFC) to be about 70% of perfect diamagnetism, which suggests bulk superconductivity. The Meissner flux expulsion (FC) is about 45% of the diamagnetic flux expulsion, a characteristic of strong flux pinning. The inset of Fig. 4a displays the 5-quadrant $M \times H$ data at $T = 2.1$ K, which suggests weak type II superconducting behavior. Figure 4b shows the estimated H_{c1} for SrBi₃, which has been calculated from the magnetic isotherms in the superconducting state, between 2.1 K - 4.5 K (inset of Fig. 4b). The value of magnetization at 2.1 K starts decreasing with increasing magnetic field, reverts the slope at 210 Oe, increases up to 790 Oe, reaches zero and saturates at an applied field of 800 Oe. Similar behaviors are observed for higher temperatures within the superconducting state, i.e., below 5.6 K. The magnetization curves confirm the type-II nature of the superconductivity with $H_{c1} = 210$ Oe and an upper critical field (H_{c2}) of about 790 Oe at 2.1 K. The small value of $H_{c2}(0)$ implies large superconducting coherence length of $\xi_0 = 615$ Å, according to $H_{c2}(0) = \Phi_0 / 2\pi\xi_0^2$ [21]. The calculated $H_c(0)$ at absolute zero temperature, from $H_c = (H_{c1}H_{c2})^{1/2}$ is 410 Oe. According to Ginzburg–Landau theory in the Meissner state, the upper critical field and thermodynamic critical field are related by $H_{c2} = 2^{1/2}\kappa H_c$. The Ginzburg–Landau parameter κ thus estimated is $1.38 > 1/2^{1/2}$, implying type-II superconductivity in SrBi₃ [21]. The penetration depth $\lambda(0)$ is calculated from the relation $\lambda(0) = \kappa\xi(0)$, resulting in 848 Å.

The temperature dependence of dc magnetization under various hydrostatic pressures up to 0.75 Pa for a BaBi₃ single crystal is shown in Fig. 5a. The measurements were carried out in ZFC protocol under $H = 10$ Oe. We define the T_c onset as the beginning of the diamagnetic response, as shown in Fig. 5a. From the $M \times T$ curve at ambient pressure, the T_c for BaBi₃ is 6 K. As the pressure increases up to 0.5 GPa, the T_c increases linearly with sharp onset transitions, up to $T_c \sim 6.6$ K. On the other hand, a broadening of the full superconducting transition appears at applied pressure 0.5 GPa, and may be due to a structural phase transition in BaBi₃ single crystal compound. The possibility of a pressure-induced structural phase transition should be further investigated with x-ray diffraction measurements under pressure. For the further applied pressure 0.75 GPa, it is observed that the T_c almost saturated at 6.6 K. Figure 5b shows the evolution of T_c

against applied pressure. Linear fitting of the data results in a positive pressure coefficient of $dT_c/dP = 1.22$ K/GPa for the BaBi₃ single crystal. The magnitude of this positive pressure coefficient is comparable to that of superconducting compounds such as LuNi₂B₂C and MgC_xNi₃ [14,15].

Figure 6a shows the temperature dependence of dc magnetization under various hydrostatic pressures up to 0.81 GPa for a SrBi₃ single crystal, measured in ZFC protocol under $H = 10$ Oe. The T_c onset at ambient pressure for SrBi₃ is 5.6 K. As the applied pressure increases the T_c of the compound decreases linearly up to 0.5 GPa with a negative pressure coefficient $dT_c/dP = -0.41$ K/GPa. Above 0.5 GPa, superconductivity decreases with a larger negative pressure coefficient $dT_c/dP = -0.68$ K/GPa. The two slopes in decreasing T_c with applied pressure can be clearly seen in Fig. 6b, and the estimated average value of dT_c/dP is -0.48 K/GPa. The superconducting volume fraction increases at the first applied pressure of 0.01 GPa, then decreases consistently for higher applied pressures. The decrease in T_c with applied pressure has been reported earlier for elemental superconductors like Sn, In, Ta, or Hg, and intermetallic superconductors like MgB₂ and BiPd [16-20].

Meanwhile, the density of states (DOS) is large enough in ABi₃ (Ba, Sr) to produce strong electron-phonon coupling [9-11], the T_c can be expressed by the McMillan formula [22] as $T_c = (\theta_D/1.45)\exp[-1.04(1+\lambda)/\{\lambda-\mu^*(1+0.62\lambda)\}]$, where θ_D is the Debye temperature, μ^* is the Coulomb pseudopotential and λ is the electron-phonon coupling constant, which can be defined as $\lambda = N(E_F)\langle I^2 \rangle / M\langle \omega^2 \rangle$, where $N(E_F)$ is the DOS at the Fermi level, $\langle I^2 \rangle$ is the average squared electronic matrix element, M is the ionic mass and $\langle \omega^2 \rangle$ is the average square phonon frequency. It is seen from the McMillan relation that the change of λ and θ_D by pressure will define the sign of dT_c/dP . It is well known that the applied pressure induces lattice stiffening and usually reduces the T_c . On the other hand, the DOS effect can increase or decrease the T_c depending on the increase or decrease of $N(E_F)$ due to applied pressure. It is clear from the McMillan formula that the dependence of T_c on θ_D is more complex than the change in λ . In general, the decrease in T_c can be understood as resulting from the θ_D increasing with applying pressure, which increases the phonon frequency as $\langle \omega^2 \rangle = 0.5\theta_D^2$ and consequently λ decreases. Therefore, the positive dT_c/dP for BaBi₃ is possibly originated from the increase of $N(E_F)$ and thus by the enhancement

of electron-phonon coupling constant λ . The negative dT_c/dP for SrBi₃ is resultant of the decrease of electron-phonon coupling constant λ due to increase in θ_D .

The temperature-dependent electrical resistivity from 2–300 K is shown in Fig. 7a for single crystal BaBi₃. The sample is metallic with resistivity decreasing linearly above $T = 40$ K, but decreasing more rapidly for $T < 40$ K, and showing a sharp superconducting transition at $T_c = 6$ K. The resistivity in the temperature range of 6–40 K displays Fermi liquid behavior, which allows to fit the resistivity relation $\rho = \rho_0 + AT^2$. The residual resistivity results in $\rho_0 = 0.15$ m Ω .cm and the impurity scattering factor in $A = 1.15$ m Ω .cm/K², which suggests that BaBi₃ is a weakly correlated system. Inset-I of Fig. 7a shows the resistivity under various magnetic fields in the superconducting transition temperature region. The sharp superconducting transitions are consistent with the increasing magnetic fields $\rho(T)|_H$ measurements and also indicative of good sample quality. The superconducting transition T_c onset and $T_c(\rho=0)$ shift towards lower temperatures with increasing applied magnetic field, as expected for a typical type-II superconductor. The estimated upper critical field is shown in Inset-II of Fig. 7a through analysis of the magnetoresistance data by selecting the 90% normal state resistivity (ρ_n) drop as the transition temperature. We estimate the orbital upper critical field, $H_{c2}(0)$, from the Werthamer-Helfand-Hohenberg (WHH) expression, i.e., $H_{c2}(0) = -0.693T_c(dH_{c2}/dT)|_{T=T_c}$ [23]. The slope is used to calculate $H_{c2}(0) = 22$ kOe by linear fitting of the $H_{c2} \times T$ data. The obtained value of $H_{c2}(0)$ is smaller than the weak coupling Pauli paramagnetic limit $H^{Pauli} = 1.82 T_c = 109.2$ kOe, which suggests a conventional superconducting mechanism for BaBi₃ [25,26].

Figure 7b presents the $\rho \times T$ measurements in the temperature range 2–300 K for a SrBi₃ single crystal. It is a very good metal with resistivity decreasing linearly for $T > 50$ K, then decreases a little more rapidly for $T_c < T < 50$ K, and shows Fermi liquid behavior fitted to the formula $\rho = \rho_0 + AT^2$. The residual resistivity is $\rho_0 = 5.3$ $\mu\Omega$.cm and the impurity scattering factor is $A = 2.7 \times 10^3$ $\mu\Omega$.cm/K², indication of electron-electron interactions in SrBi₃. The sharp superconducting transition at 5.9 K is clearly shown in $\rho(T)|_H$ curves in the upper inset of Fig 7b. The T_c is suppressed with applied magnetic field, and the suppression rate at very low fields, up to just 3.0 kOe, indicates weak type-II superconductivity in SrBi₃. The lower inset of Fig. 7b shows the estimated upper critical field for SrBi₃. We take the 90% criteria of normal state

resistivity drop point as the transition temperature to calculate the orbital upper critical field, $H_{c2}(0)$, from the WHH equation, i.e., $H_{c2}(0) = -0.693T_c(dH_{c2}/dT)|_{T=T_c}$ [23]. The slope obtained from linear fitting $H_{c2} \times T$ data is used to calculate $H_{c2}(0) = 2.9$ kOe. The value of $H_{c2}(0)$ is much smaller than the weak coupling Pauli paramagnetic limit $H^{Pauli} = 1.82 T_c = 109$ kOe for SrBi₃ [24,25].

The specific heat data divided by temperature (C_p/T) $\times T$ data for a BaBi₃ single crystal, with and without an applied magnetic field of 50 kOe, is shown in Fig. 8a. The specific heat is sensitive to low temperature electronic excitations and different gap symmetries have different densities of electronic states, i.e., it gives information about the ground state of the system. The lower inset of Fig. 8a shows the heat capacity in applied field 50 kOe, which is best fit to the relation $C_p(T) = \gamma T + \beta T^3 + \delta T^5$ (solid red line). The evaluated specific heat capacity coefficients are $\gamma = 3.2$ mJ/mol \cdot K², $\beta = 0.155$ mJ/mol \cdot K⁴ and $\delta = 0.00581$ mJ/mol \cdot K⁶, which results in a Debye temperature $\theta_D = (234zR/\beta)^{1/3} = 171$ K. Here $z = 4$ is the number of atoms in the BaBi₃ unit cell, and the Rydberg constant $R = 8.314$ J/mol \cdot K is the term γT is the normal state electronic contribution and βT^3 and δT^5 are the lattice contributions to the specific heat. The upper inset of Fig. 8a shows the electronic contribution of specific heat C_e/T as a function of temperature. Here $C_e(T) = C_p - \beta T^3 - \delta T^5$, i.e., the lattice contribution subtracted from the total C_p . The observed specific heat jump $\Delta C_e/\gamma T_c = 1.05$ is lower than the BCS theory value of 1.43, suggesting weak coupling superconductivity in BaBi₃. Our value is very similar to that obtained by Haldolaarachchige *et al.* [9] for their BaBi₃ single crystalline sample.

Figure 8b presents the temperature-dependent specific heat C_p/T for the SrBi₃ single crystal, with and without an applied magnetic field of 50 kOe. The specific heat capacity coefficients are calculated as $\gamma = 6.5$ mJ/mol \cdot K², $\beta = 0.124$ mJ/mol \cdot K⁴ and $\delta = 0.00581$ mJ/mol \cdot K⁶, through the relation $C_p(T) = \gamma T + \beta T^3 + \delta T^5$ (solid red line) by fitting the heat capacity data in applied field of 50 kOe seen in the lower inset. The Debye temperature is $\theta_D = (234zR/\beta)^{1/3} = 180$ K. The upper inset of Fig. 8b shows the electronic contribution of specific heat C_e/T as a function of temperature and the observed specific heat jump $\Delta C_e/\gamma T_c = 2.08$ is higher than the BCS theory value of 1.43, suggesting SrBi₃ as a strong coupled superconductor. Our result is in

reasonably good agreement with the previous reported values of 2.7 by Kempf *et al.* and 2.17 by Shao *et al.* [11, 26].

In summary, the single crystalline BaBi₃ and SrBi₃ compounds studied in this work have shown different crystal structures, respectively tetragonal with space group *P4/mmm* and cubic with space group *Pm-3m*. The difference in lattice parameters $a = 5.06(1) \text{ \AA}$ and $c = 5.13(2) \text{ \AA}$ is relatively small, i.e., BaBi₃ crystallizes in a distorted AuCu₃ type structure, while SrBi₃ crystallizes in the AuCu₃ structure with lattice parameter $a = 5.05(3) \text{ \AA}$. Both compounds have quite different values of superconducting parameters in the scenario of conventional type-II superconductivity, as summarized in Table 1. The hydrostatic pressure studies for BaBi₃ and SrBi₃ single crystals show a positive pressure coefficient of $dT_c/dP = 1.22 \text{ K/GPa}$ and a negative pressure coefficient $dT_c/dP = -0.48 \text{ K/GPa}$, respectively. Heat capacity studies suggest that BaBi₃ is a weak coupled superconductor, whereas SrBi₃ is a strongly coupled superconductor.

Acknowledgements

The authors thank P.G. Pagliuso for access to the GPOMS PPMS used for the resistivity measurements. We are thankful to Dr. V. P. S. Awana (CSIR-National Physical Laboratory, New Delhi, India) for his valuable discussions and for reviewing the manuscript. This work is supported by Brazilian agencies FINEP, CNPq and FAPESP (Grant Nos. 2011/19924-2, 2015/15403-9).

References:

1. Y. Xia, D. Qian, D. Hsieh, L. Wray, A. Pal, H. Lin, A. Bansil, D. Grauer, Y. S. Hor, R. J. Cava and M. Z. Hasan, *Nature Phys.* **5**, 398 (2009).
2. Y. L. Chen, J. G. Analytis, J.-H. Chu, Z. K. Liu, S.-K. Mo, X. L. Qi, H. J. Zhang, D. H. Lu, X. Dai, Z. Fang, S. C. Zhang, I. R. Fisher, Z. Hussain and Z.-X. Shen, *Science* **325**, 178 (2009).
3. Y. Mizuguchi, H. Fujihisa, Y. Gotoh, K. Suzuki, H. Usui, K. Kuroki, S. Demura, Y. Takano, H. Izawa and O. Miura, *Phys. Rev. B* **86**, 220510(R) (2012).
4. S. K. Singh, A. Kumar, B. Gahtori, Shruti; G. Sharma, S. Patnaik and V. P. S. Awana, *J. Am. Chem. Soc.* **134**, 16504 (2012).
5. V.P.S. Awana, A. Kumar, R. Jha, S. K. Singh, A. Pal, Shruti, J. Saha and S. Patnaik, *Solid State Communications* **157**, 21 (2013).

6. S. Demura, Y. Mizuguchi, K. Deguchi, H. Okazaki, H. Hara, T. Watanabe, S. J. Denholme, M. Fujioka, T. Ozaki, H. Fujihisa, Y. Gotoh, O. Miura, T. Yamaguchi, H. Takeya and Y. Takano, *J. Phys. Soc. Jpn.* **82**, 033708 (2013).
7. R. Jha, A. Kumar, S. K. Singh and V. P. S. Awana, *JOSC* **26**, 499 (2013).
8. B. T. Matthias and J. K. Hulm, *Phys. Rev.* **87**, 799 (1952).
9. N. Haldolaarachchige, S. K. Kushwaha, Q. Gibson and R. J. Cava, *Supercond. Sci. Technol.* **27**, 105001 (2014).
10. M. Kakihana, H. Akamine, T. Yara, A. Teruya, A. Nakamura, T. Takeuchi, M. Hedou, T. Nakama, Y. Ōnuki and H. Harima, *J. Phys. Soc. Jpn.* **84**, 124702 (2015).
11. D. F. Shao, X. Luo, W. J. Lu, L. Hu, X. D. Zhu, W. H. Song, X. B. Zhu and Y. P. Sun, *Sci. Rep.* **6**, 21484 (2016).
12. A. Iyo, Y. Yanagi, T. Kinjo, T. Nishio, I. Hase, T. Yanagisawa, S. Ishida, H. Kito, N. Takeshita, K. Oka, Y. Yoshida and H. Eisaki, *Sci. Rep.* **5**, 10089 (2015).
13. M. Monteverde, M. Núñez-Regueiro, N. Rogado, K. A. Regan, M. A. Hayward, T. He, S. M. Loureiro and R. J. Cava, *Science* **292**, 75 (2001).
14. B. Lorenz, R. L. Meng and C. W. Chu, *Phys. Rev. B* **64**, 012507 (2001).
15. H. D. Yang, S. Mollah, W. L. Huang, P. L. Ho, H. L. Huang, C.-J. Liu, J.-Y. Lin, Y.-L. Zhang, R.-C. Yu and C.-Q. Jin, *Phys. Rev. B* **68**, 092507 (2003).
16. H. Schmidt and H. F. Braun, *Physica C* **229**, 315 (1994).
17. M. Ishizuka, M. Iketani and S. Endo, *Phys. Rev. B* **61**, R3823(R) (2000).
18. R. Jha, R. Goyal, P. Neha, V. K. Maurya, A. K. Srivastava, A. Gupta, S. Patnaik and V. P. S. Awana, *Supercond. Sci. Technol.* **29**, 025008 (2016).
19. L. D. Jennings and C. A. Swenson, *Phys. Rev.* **112**, 31 (1958).
20. C. Nirmala Louis and K. Iyakutti, *Phys. Rev. B* **67**, 094509 (2003).
21. M. Zehetmayer, *Supercond. Sci. Technol.* **26**, 043001 (2013).
22. W. L. McMillan, *Phys. Rev.* **167**, 331 (1968).
23. N. R. Werthamer, E. Helfand and P. C. Hohenberg, *Phys. Rev.* **147**, 295 (1966).
24. A. M. Clogston, *Phys. Rev. Lett.* **9**, 266 (1962).
25. B. S. Chandrasekhar, *Appl. Phys. Lett.* **1**, 7 (1962).
26. B. Kempf, B. Elschner, P. Spitzli, and Ø. Fischer, *Phys. Rev. B* **17**, 2163 (1978).

Table 1. Summary of the superconducting parameters of ABi_3 (A=Ba, Sr) single crystals.

Parameters	Units	BaBi ₃	SrBi ₃
T_c	K	6.0	5.6
$H_{c1}(0)$	Oe	1710	210
$H_{c2}(0)$	Oe	14710	790
$H_c(0)$	Oe	5015	410
ξ	Å	149	615
λ	Å	309	848
κ	Å	2.07	1.38
dT_c/dP	K/GPa	1.22	-0.48
$\Delta C_e/\gamma T_c$		1.05	2.08
Θ_D	K	171	180

Figure captions

Figure 1: Photos of the as-grown single crystals of (a) BaBi₃ and (b) SrBi₃.

Figure 2: (a) Room temperature X-ray diffraction patterns of ABi₃ (A=Ba,Sr) single crystalline clusters (red open circles), Rietveld refinements (black solid line) and differences (blue solid line). (b) Schematic representation of the crystal structure of ABi₃ (A=Ba, Sr).

Figure 3: (a) Temperature dependence of the dc magnetic susceptibility in ZFC and FC modes for BaBi₃ single crystal. The inset is the isothermal magnetization loop at 2.1 K. (b) Lower critical field H_{c1} as a function of normalized temperature T/T_c . The red solid line represents the fitting of the equation $H_{c1}(T) = H_{c1}(0)[1-(T/T_c)^2]$. The inset shows the initial (ZFC) isothermal magnetization branches at different temperatures.

Figure 4: (a) Temperature dependence of the dc magnetic susceptibility in ZFC and FC modes for SrBi₃ single crystal. The inset is the isothermal magnetization loop at 2.1 K. (b) Lower critical field H_{c1} as a function of normalized temperature T/T_c . The red solid line represents the fitting of the equation $H_{c1}(T) = H_{c1}(0)[1-(T/T_c)^2]$. The inset shows the initial (ZFC) isothermal magnetization branches at different temperatures.

Figure 5: (a) dc magnetic susceptibility as a function of temperature in ZFC mode for a BaBi₃ single crystal under various hydrostatic pressures (0-0.75 GPa). (b) T_c^{onset} vs. applied pressure for the BaBi₃ single crystal.

Figure 6: (a) dc magnetic susceptibility as a function of temperature in ZFC mode for a SrBi₃ single crystal under various hydrostatic pressures (0-0.81 GPa). (b) T_c^{onset} vs. applied pressure for the SrBi₃ single crystal.

Figure 7: (a) Temperature dependence of the electrical resistivity of a BaBi₃ single crystal, including a low- T curve fitting of the relation $\rho = \rho_0 + AT^2$. Inset-I shows $\rho(T)$ under various applied magnetic fields. Inset-II shows the upper critical field (H_{c2}) as a function of

temperature and the red solid line is data fit of the WHH expression (see text). (b) Temperature dependence of the electrical resistivity of a SrBi₃ single crystal, including a low- T curve fitting of the relation $\rho = \rho_0 + AT^2$. Inset-I shows $\rho(T)$ under various applied magnetic fields. Inset-II shows the upper critical field (H_{c2}) as a function of temperature and the red solid line is data fit of the WHH expression.

Figure 8: (a) Heat capacity C_p/T vs. T of a BaBi₃ single crystal in the temperature range 4-8 K. The lower inset shows heat capacity under applied field of 50 kOe fitted by $C_p(T) = \gamma T + \beta T^3 + \delta T^5$. The upper inset shows the electronic part C_e/T vs. T around the transition. (b) Heat capacity C_p/T vs. T of a SrBi₃ single crystal in the temperature range 4-8 K. The lower inset shows heat capacity under applied field of 50 kOe fitted by $C_p(T) = \gamma T + \beta T^3 + \delta T^5$. The upper inset shows the electronic part C_e/T vs. T around the transition.

Figure 1.

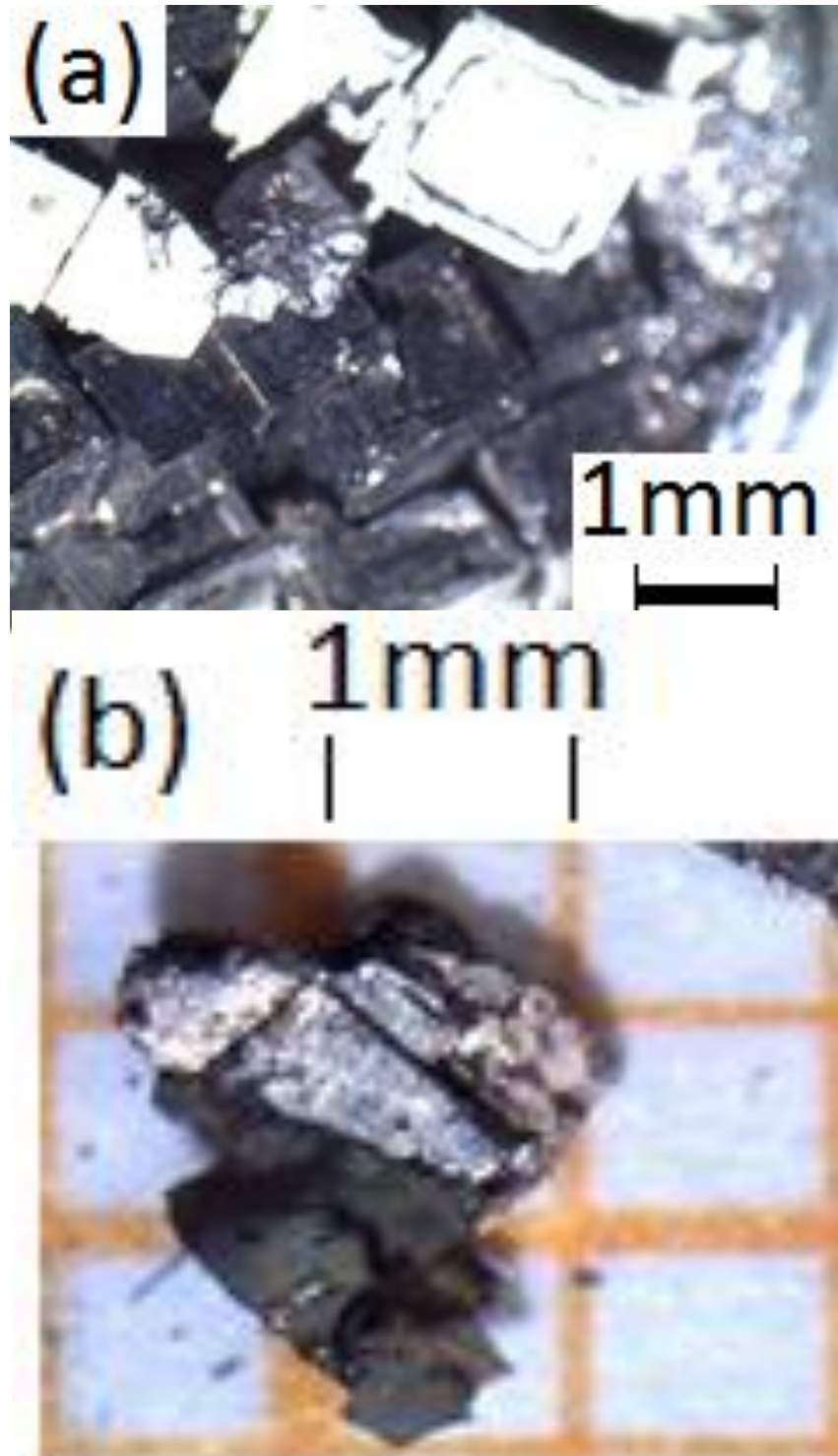


Figure 2.

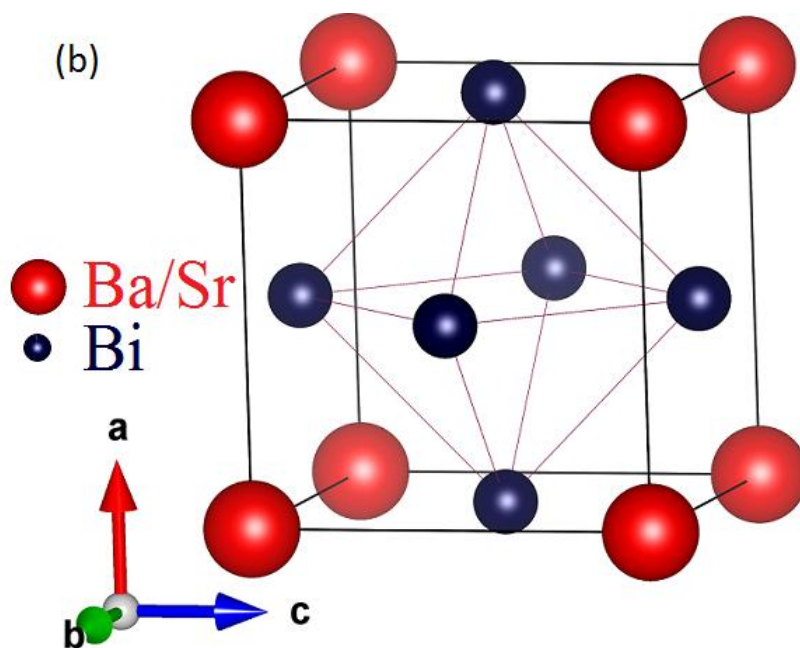
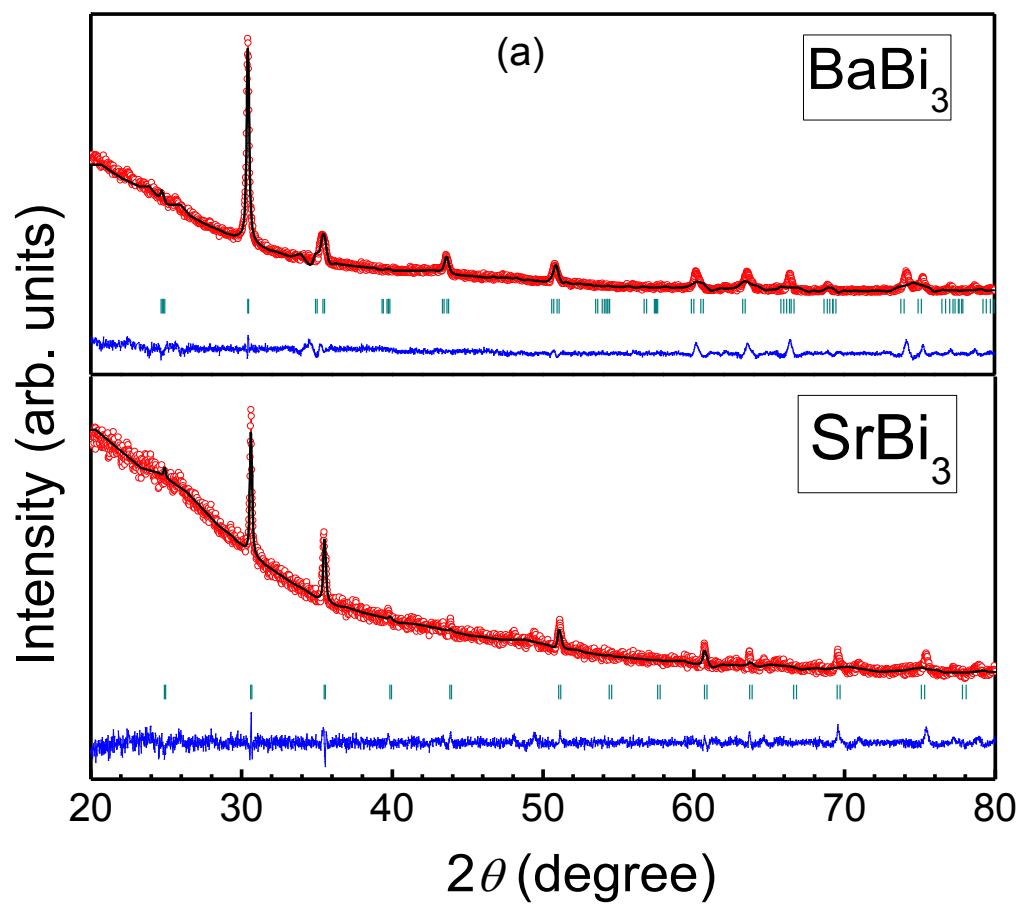


Figure 3.

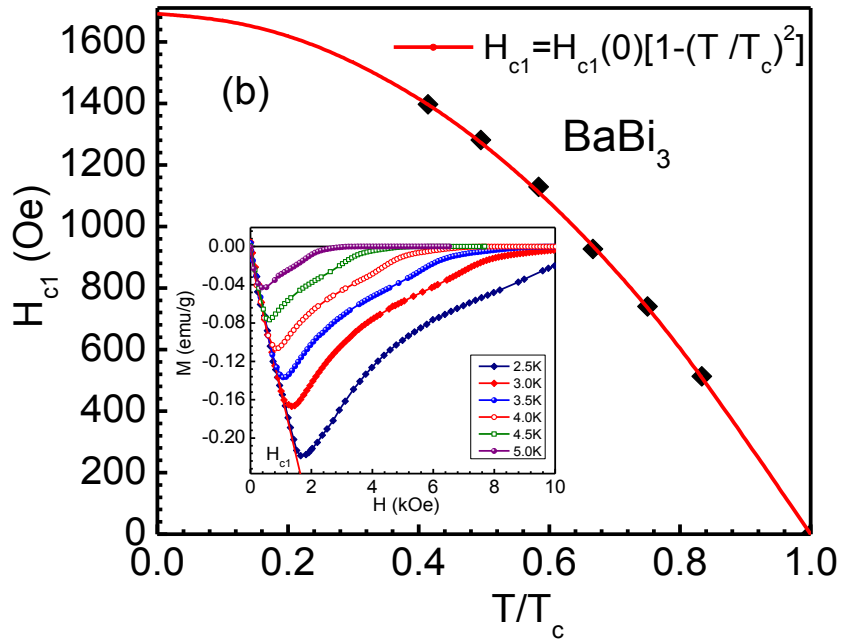
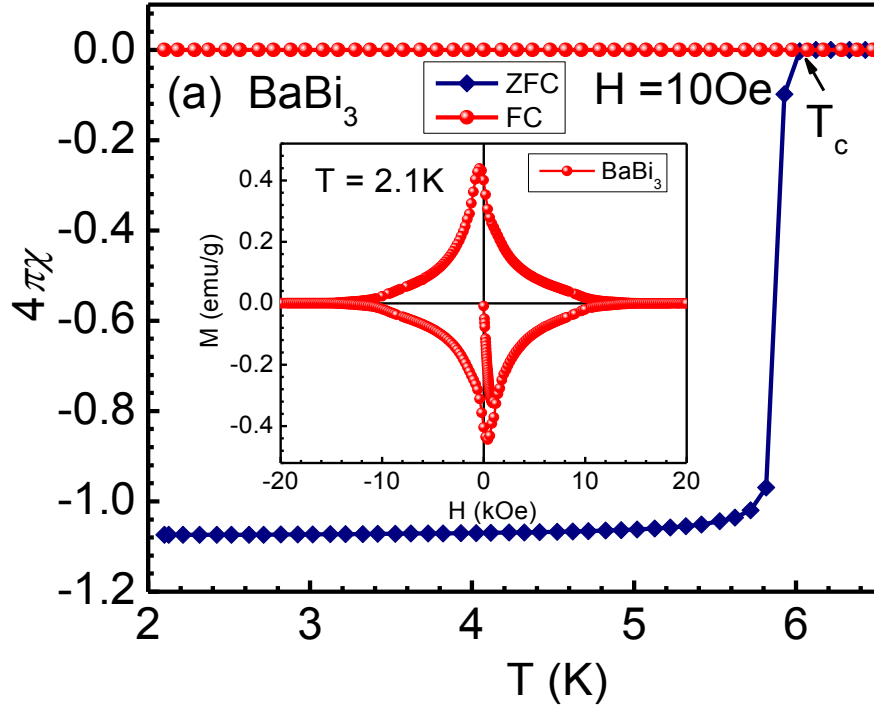


Figure 4.

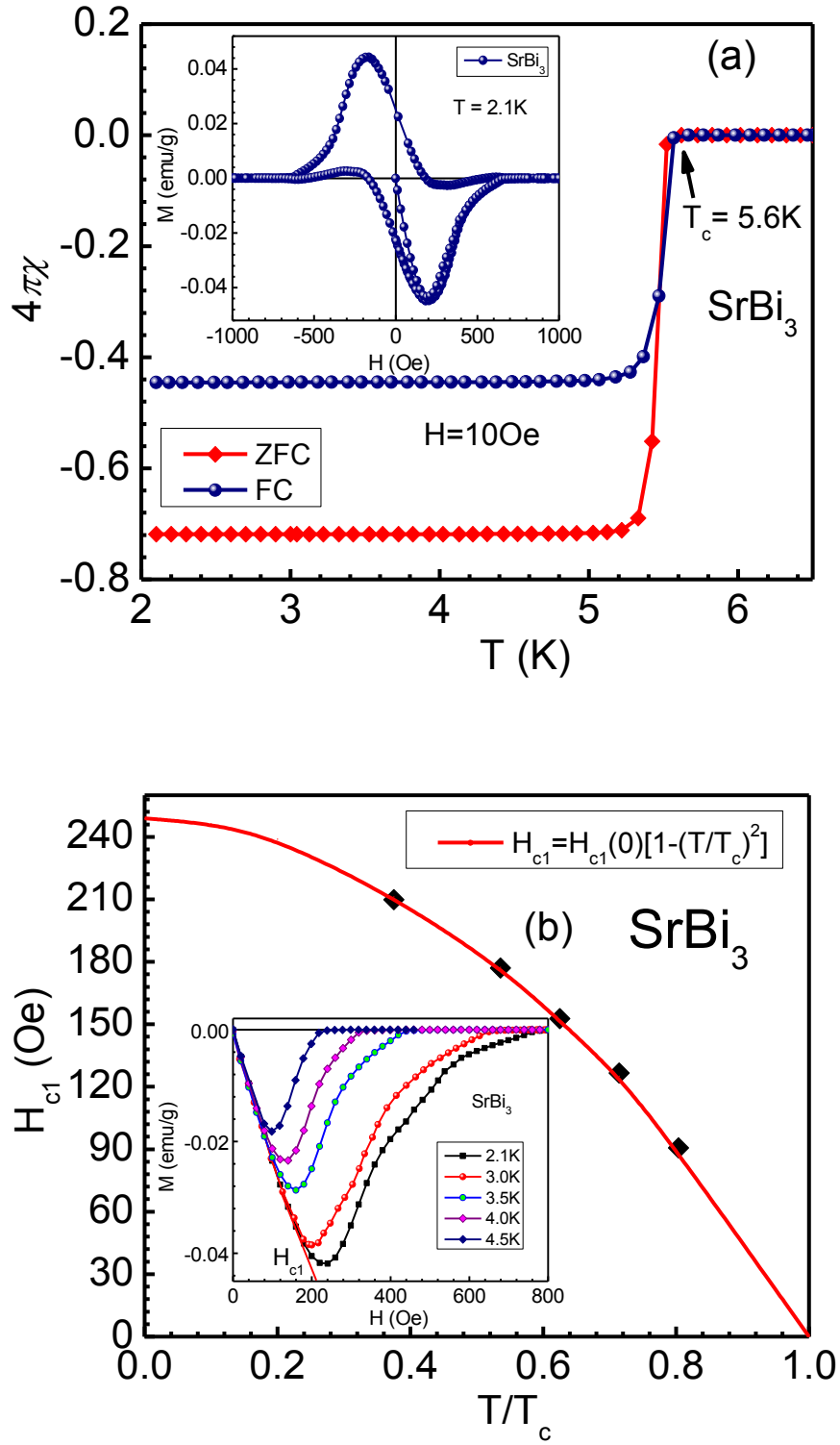
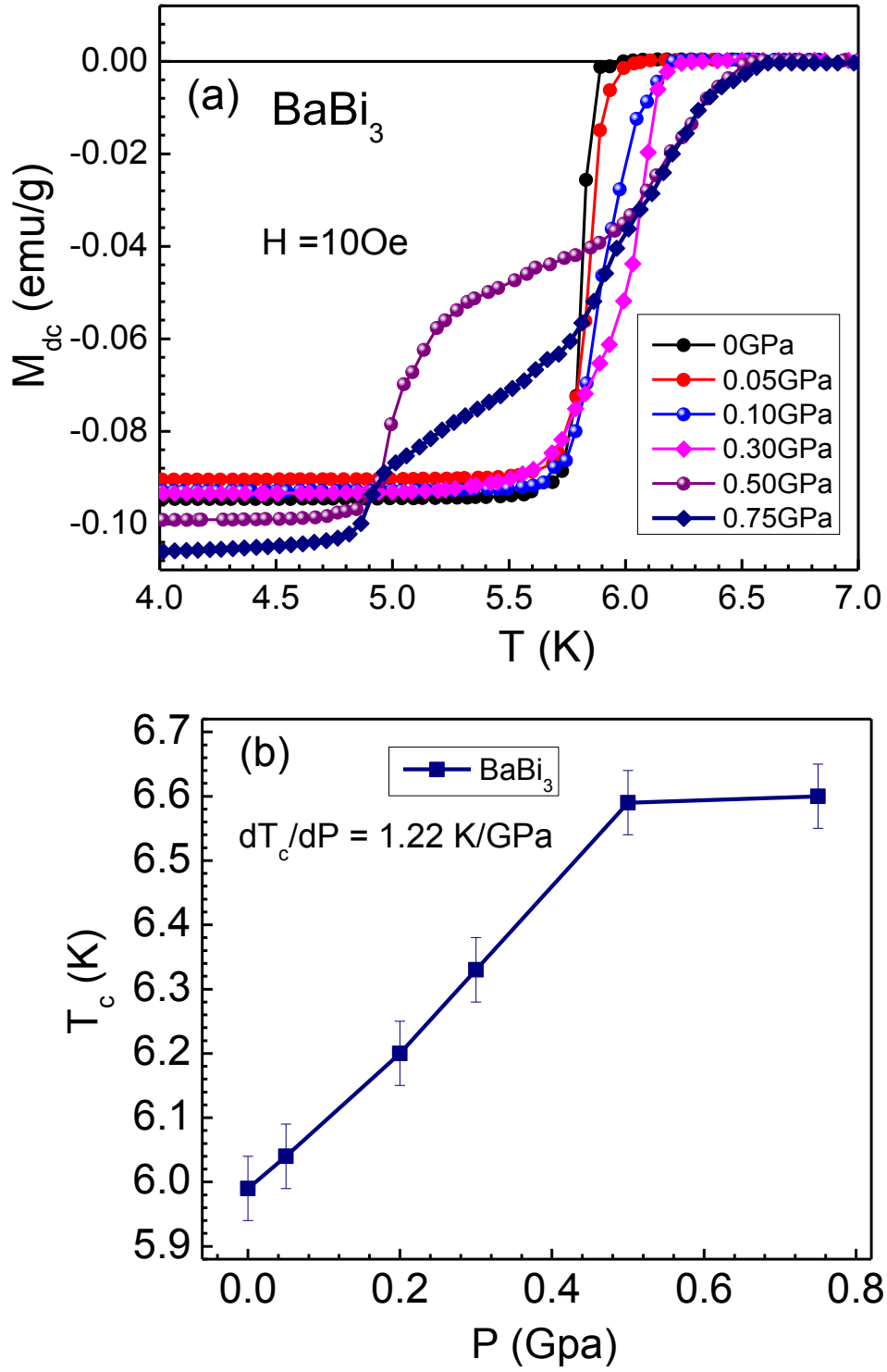


Figure 5.



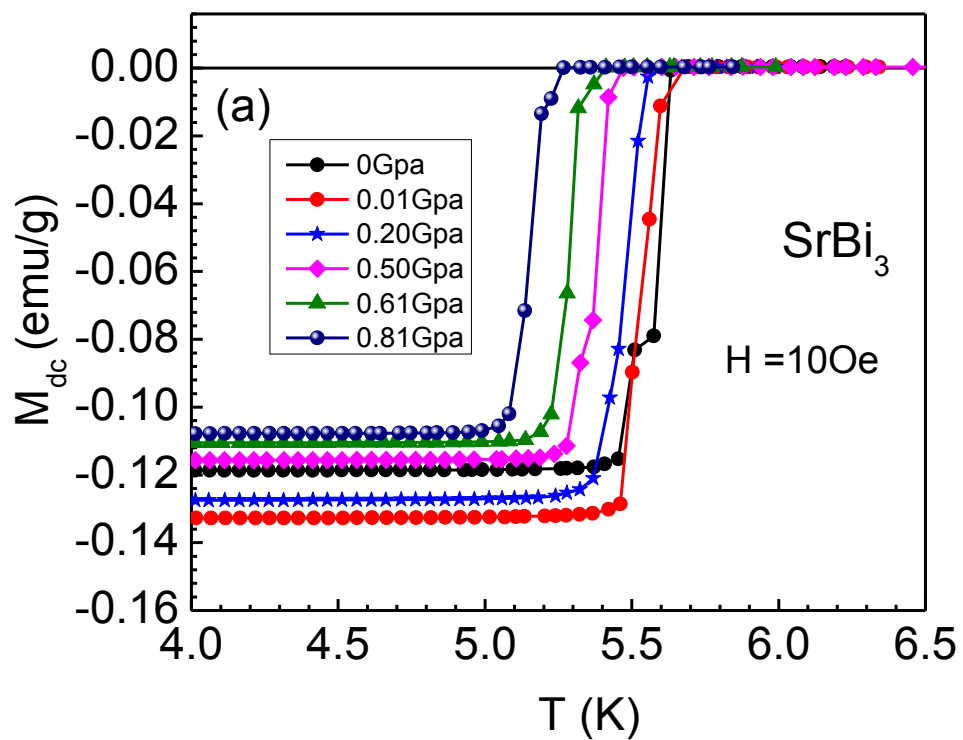


Figure 6.

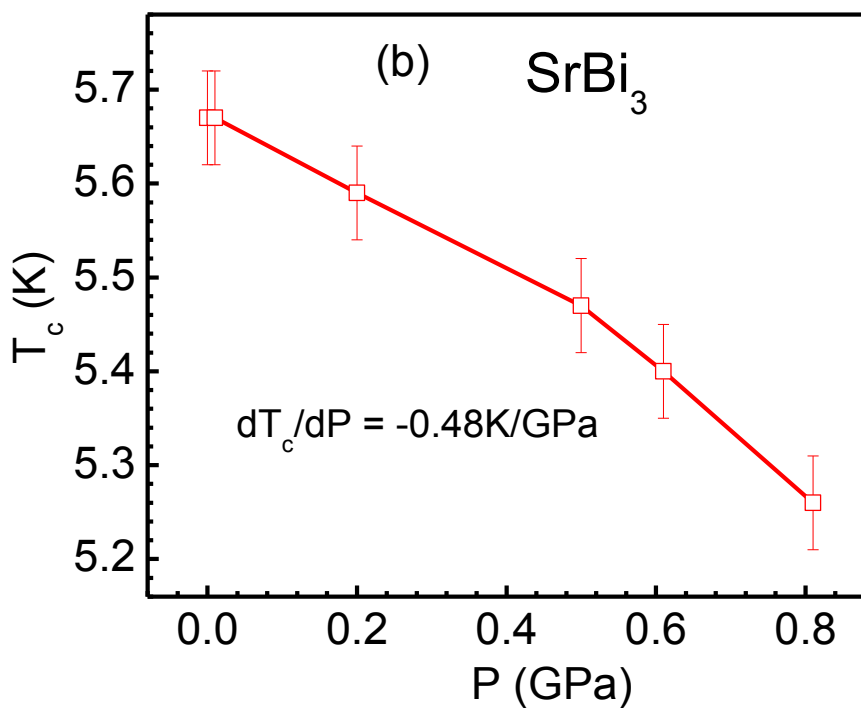


Figure 7.

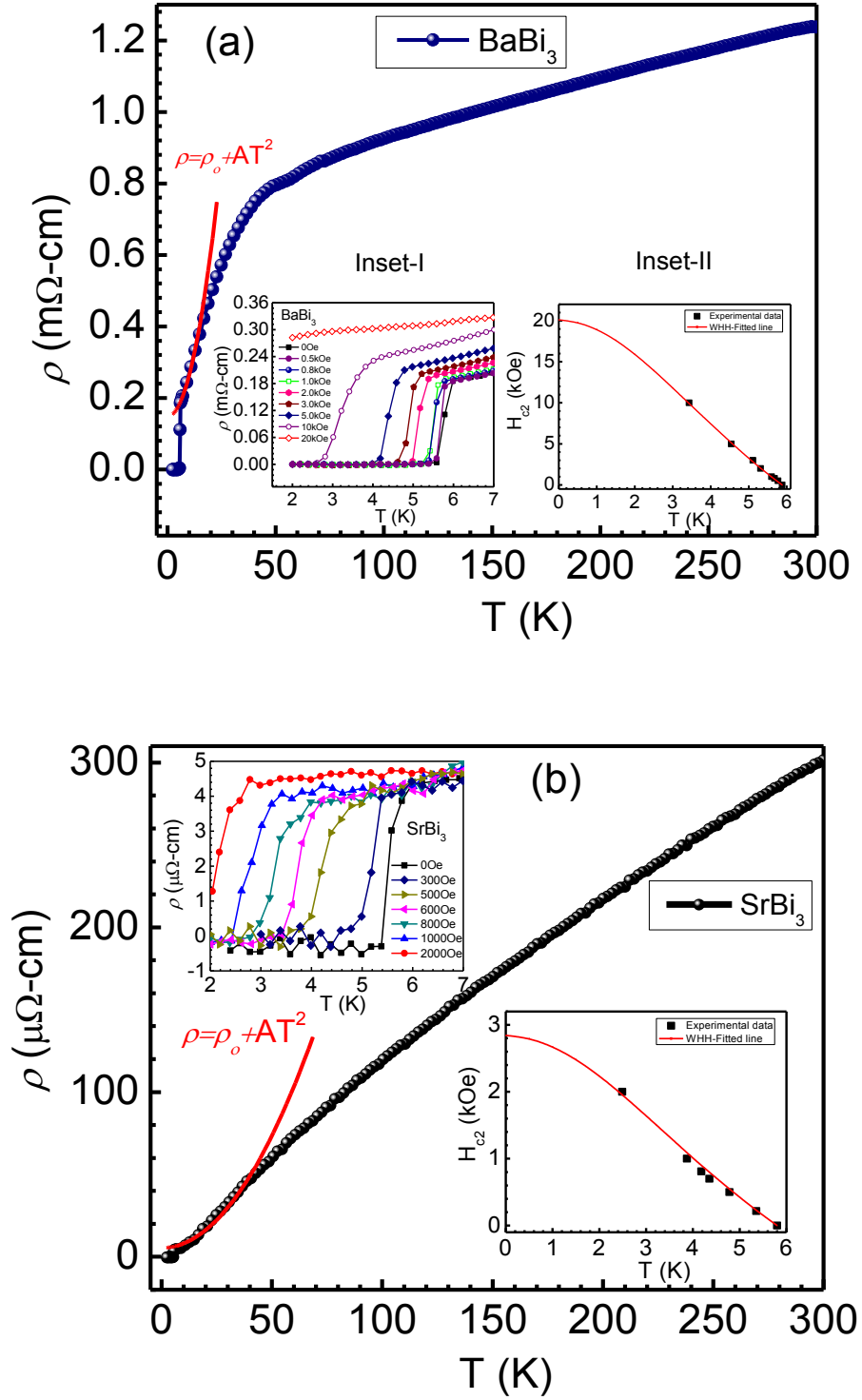


Figure 8.

